Improving country-wide individual tree detection using local maxima methods based on statistically modeled forest structure information

Christoph Schaller [a],[*], Christian Ginzler [b], Emiel van Loon [c], Christine Moos [a], Arie C. Seijmonsbergen [c], Luuk Dorren [a]

[a] *Bern University of Applied Sciences - HAFL, Länggasse 85, 3052, Zollikofen, Switzerland*
[b] *The Swiss Federal Institute for Forest, Snow and Landscape Research WSL, Zürcherstrasse 111, 8903, Birmensdorf, Switzerland*
[c] *University of Amsterdam UVA - IBED, Sciencepark 904, 1098 XH, Amsterdam, The Netherlands*

ARTICLE INFO	ABSTRACT
	Individual tree detection using airborne laser scanning (ALS) can provide relevant data to complement forest inventory data. Local Maxima-based (LM) methods for individual tree detection are suitable for applications over large extents, but their performance depends on the type of pre-processing of the input data, as well as forest structure and composition. We developed a model that improves LM through statistical modeling using prior knowledge about forest structure. The model selects the optimal canopy height model (CHM) pre-processing filters based on forest structure variables like the dominant canopy height and degree of cover derived from ALS data, the dominant leaf type derived from Sentinel data, and terrain metrics. The model performance was evaluated by assessing tree detection errors for the canopy stem count in National Forest Inventory (NFI) plots in Switzerland (n=5254). For plots with point densities of more than 15 points per square meter and, at most, 6 years between ALS acquisition and inventory (n=2676), the results showed a mean absolute error of 61 stems per ha compared to 174 stems per ha when detecting trees using an unprocessed CHM. The model showed a stable performance for different dominant leaf types (broadleaved-dominated, mixed, coniferous-dominated) and for different degrees of cover. We consider the developed model to be suitable for applications that require data on forest structure or individual tree positions and heights over large areas.

1. Introduction

Forest ecosystems simultaneously provide multiple services varying from production, socio-cultural services, such as recreation, and regulation services, such as natural hazard risk reduction, water and temperature regulation, biodiversity, and carbon sequestration (Harrison et al., 2010; Pohjanmies et al., 2017). To manage forests and to quantify their function performance, data on forest structure (tree positions, tree heights, layering, and stem diameters) and tree-species distribution are required. Traditionally, such data have been acquired by cost- and labor-intensive sample-based forest inventories using terrestrial sample plots (Hyyppä et al., 2000; Kangas et al., 2006; Hyyppä et al., 2008; Zhen et al., 2016). Today, remote sensing has become standard to obtain spatially explicit data for complementing plot-based inventories over large areas in a mostly automated and cost-efficient manner (Breidenbach and Astrup, 2014; Eysn et al., 2015; Zhen et al., 2016).

Both data from passive remote sensing sensors (e.g. multispectral satellite imagery) and active sensors (e.g. light detection and ranging LiDAR and synthetic aperture radar SAR) are used for forest inventory purposes (Hyyppä et al., 2008; Zhen et al., 2016). Especially, the improvement in sensors and data availability for airborne laser scanning (ALS) increased research and use of active remote sensing data (Zhen et al., 2016). Tree detection can be performed in the point cloud, a rasterized canopy height model (CHM) interpolated from those points, or a combination of the two (Hyyppä et al., 2008; Koch et al., 2014; Zhen et al., 2016; Hui et al., 2022). Recent research on tree detection focuses on detection in point clouds, the use of unmanned aerial vehicle-based data, and deep learning-based detection algorithms (e.g. Williams et al., 2020; Kukkonen et al., 2021; Michałowska and Rapiński, 2021; Osco et al., 2021; Sparks et al., 2022; Luo et al., 2022). However, despite advances in computing efficiency, detection methods based on point clouds remain only feasible for single plots or smaller areas (i.e., on

---

average several ha (e.g. Eysn et al., 2015; Wallace et al., 2016; Zhou et al., 2018), up to several 100 ha (e.g. Kolendo et al., 2021). For individual tree detection over several 100,000 ha, methods based on CHM remain the most feasible due to their computational efficiency compared to cloud-based methods (Zhen et al., 2016; Michałowska and Rapiński, 2021).

Local Maxima-based (LM) methods for individual tree detection based on CHM are frequently used and have shown good results in benchmark studies (Kaartinen et al., 2012; Eysn et al., 2015; Vandendaele et al., 2021; Xu et al., 2021; Sparks et al., 2022). For LM methods, detection parameters – like raster cell size, degree of smoothing or filtering, horizontal and/or vertical exclusion criteria, and the detection window – influence their performance. Thus, the adjustment of these detection parameters based on the forest structure can considerably improve the results (Koch et al., 2014; Eysn et al., 2015; Zhen et al., 2016; Mielcarek et al., 2018; Kolendo et al., 2021). In addition, LM methods are often used as sub-step in tree segmentation both in CHM and point clouds (Hyyppä et al., 2008; Vauhkonen et al., 2012; Williams et al., 2020). Besides tree height and position segmentation can provide additional information like crown size and shape or serve to reduce over-detection (Kaartinen et al., 2012; Koch et al., 2014; Zhen et al., 2016; Williams et al., 2020; Sparks et al., 2022).

The objective of this study is to improve a CHM-based LM individual tree detection method for a country-wide application in Switzerland with heterogeneous forest structures through statistical modeling using prior knowledge about forest structure and dominant leaf type. To achieve this, we developed a hybrid model, which combines linear regression models of tree detection errors based on forest structure variables with a rule-based model to select different CHM pre-processing filters. We evaluated the performance of our hybrid model by assessing tree detection errors using National Forest Inventory (NFI) data.

2. Materials

2.1. Input data

The canopy height model (CHM) is based on the most recent ALS data covering the entire country (total area 41285 km^2; forest area equals 32% of the country or 1.31 Mha). These ALS data are available either from the Federal Office of Topography (swisstopo) (Swisstopo, 2021c) or the cantons. The average point density of the LiDAR data shows varying values (Table 1), but most of the 26 cantons have at least 15 points m^{-2} on average. Data from the cantons Grisons (GR), Jura (JU), and Valais (VS) have lower point densities since they have not been updated since 2006.

As an additional input we used the current 2018 version of the 10 m cell size dominant leaf type (DLT) raster (Waser and Ginzler, 2018) derived from Sentinel data (c.f. Waser et al., 2021). Finally, the digital height model DHM25 (Swisstopo, 2021a) with a cell size of 25 m was used to derive terrain metrics for the reference plots.

2.2. Reference data

Data from inventory plots of the fourth Swiss NFI (Brändli et al., 2020) were used as reference data for the study. The inventory surveyed forest sample plots in a raster with a mesh size of 1.4 km across the whole of Switzerland between 2009 and 2017 (Brändli et al., 2020). As shown in Fig. 1, the plots were divided into an inner circle (1) of 200 m^2 (radius = 7.98 m) and an outer circle (2) of 500 m^2 (radius = 12.62 m) (Fischer and Traub, 2019). Every tree with a diameter at breast height (DBH; measured at a height of 1.3 m above the highest ground level at the tree bottom) larger than 12 cm was recorded within the inner circle, and every tree with a DBH >36 cm was recorded within the perimeter delimited by the outer circle (Fischer and Traub, 2019). The top height of the stands surrounding the NFI plot is derived from the average height of the 100 trees with the biggest DBH per

Table 1
LiDAR data used for creating the CHM.

Canton	Year of data acquisition	Point density of all returns [m^{-2}]
AG	2020	17.5
AI	2018	20.1
AR	2018	23.9
BE	2011/2012/2013	14.1
BL	2018	50.2
BS	2018	39.5
FR	2019	16.2
GE	2019	10.7
GL	2017	31.4
GR	2003	2.1
JU	2006	3.0
LU	2020	15.8
NE	2018	14.9
NW	2019	24.8
OW	2019	23.1
SG	2017	24.0
SH	2018	19.9
SO	2019	45.1
SZ	2017	26.7
TG	2017	15.8
TI	2019	25.4
UR	2019	23.0
VD	2018/2019	17.5
VS	2001/2005	1.6
ZG	2018	17.8
ZH	2018	17.5

hectare (Fischer and Traub, 2019). Based on the top height, the trees are categorized as belonging to the upper (>2/3 top height), middle (between 1/3 and 2/3 top height), or lower (<1/3 top height) layer of the canopy (Brändli et al., 2020).

Our reference data included 5254 plots across Switzerland (see Fig. 2) with the coordinates of each plot center and the number of living standing trees per plot. With altitudes ranging from 195 m to 2243 m above sea level the plots span the altitudinal zones from the colline to the alpine belt and encompass the forest profiles and main tree species in Swiss forests (c.f. Rigling and Schaffer, 2015). Only the trees within the upper layer of the canopy were selected as reference data, since they are potentially detectable by LM methods in a CHM.

3. Methods

The methodology applied in this study is divided into four stages (Fig. 3). During data processing in stage 1, input data were prepared including the ALS-derived CHM and the reference data per inventory plot. In stage 2, forest structure and terrain characteristic variables were derived from the input data. During stage 3, individual trees were detected using an LM method in combination with different pre-processing filters. The dataset resulting from stages 2 and 3 was split into calibration data (80%) for model training and validation data (20%) for analyzing the model performance in stage 4. The workflow code is available in an online repository (Schaller and Dorren, 2023).

3.1. Data pre-processing

For the preparation of the CHM (step S1.1 in Fig. 3), a 1 m cell size raster covering Switzerland was generated using the ALS data. First, the raw point data were normalized. In case there were existing ASPRS (American Society for Photogrammetry and Remote Sensing) classes, the class 'ground points' was used to determine the terrain elevation. Otherwise, the 2021 version of the swissAlti3D digital elevation model from swisstopo was used (Swisstopo, 2021b). During normalization, the height above ground was calculated for each point. In absence of the ASPRS classification for buildings, the footprints of building data from the swisstopo Topographic Landscape Model (TLM) were used to classify building points. From the normalized points, raster
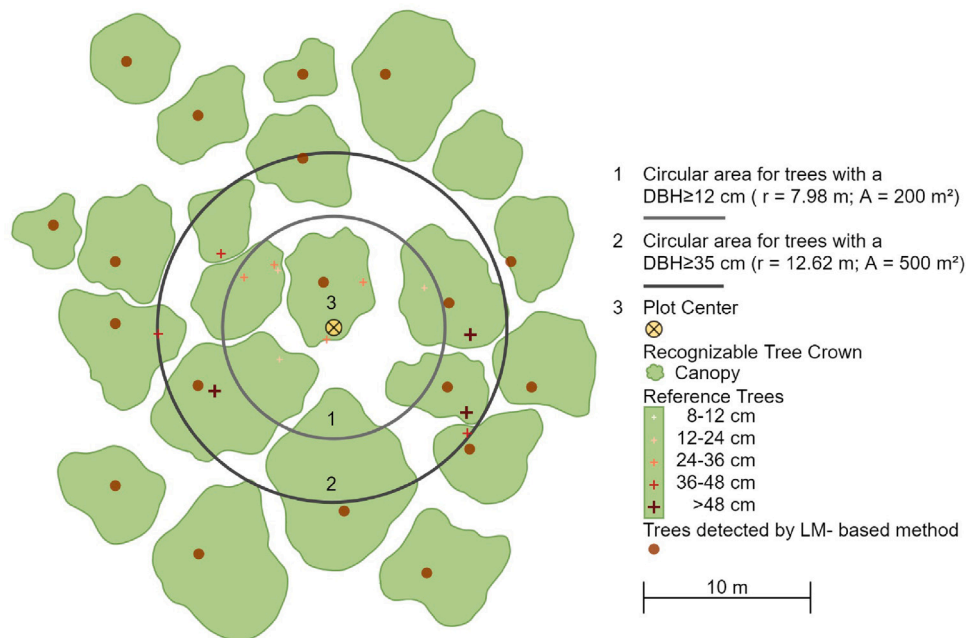
Fig. 1. Schematic representation of an NFI sample plot including circular plot boundaries, plot center, positions of reference, and detected trees.
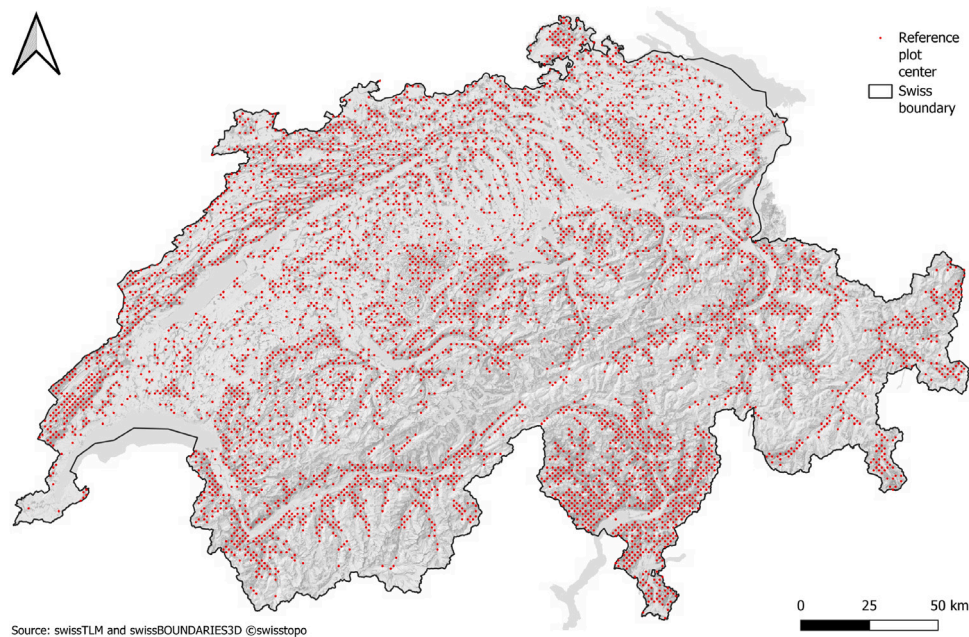

Fig. 2. Map showing the distribution of the NFI sample plots across Switzerland.

data with a cell size of 1 m were calculated with the grid function of LAStools. All points except for the point class 'building' were used. The highest LiDAR point was used for each raster cell. Gaps were linearly interpolated.

3.2. Calculation of variables

In the third stage, the variables listed in Table 2, which are used as input for the hybrid model, were calculated based on the pre-processed input data. The variables were calculated by aggregating the inputs to a 25 m cell size raster using different aggregation functions. For each NFI plot, the values from the raster cell containing the plot center were added to the reference data. The forest structure variables are based on the CHM (resampled to 1.5 m with a maximum function to

provide basic smoothing) and DLT rasters (Rosset, 2021) (step S2.1 in Fig. 3). Additional variables relating to the CHM roughness and number of peaks were derived directly from the 1 m cell size raster. Terrain characteristic variables were derived from the DHM25 digital terrain model using GDAL (Geospatial Data Abstraction Library GDAL/OGR contributors, 2021).

3.3. Local maxima-based tree detection

The actual tree detection was performed using a Python (van Rossum and Drake, 2009) implementation of a LM algorithm using a CHM (Schaller and Contributors, 2022). Circular windows were used to determine whether the center cell of the window is a local maximum or not (i.e., whether the cell is higher than the surrounding
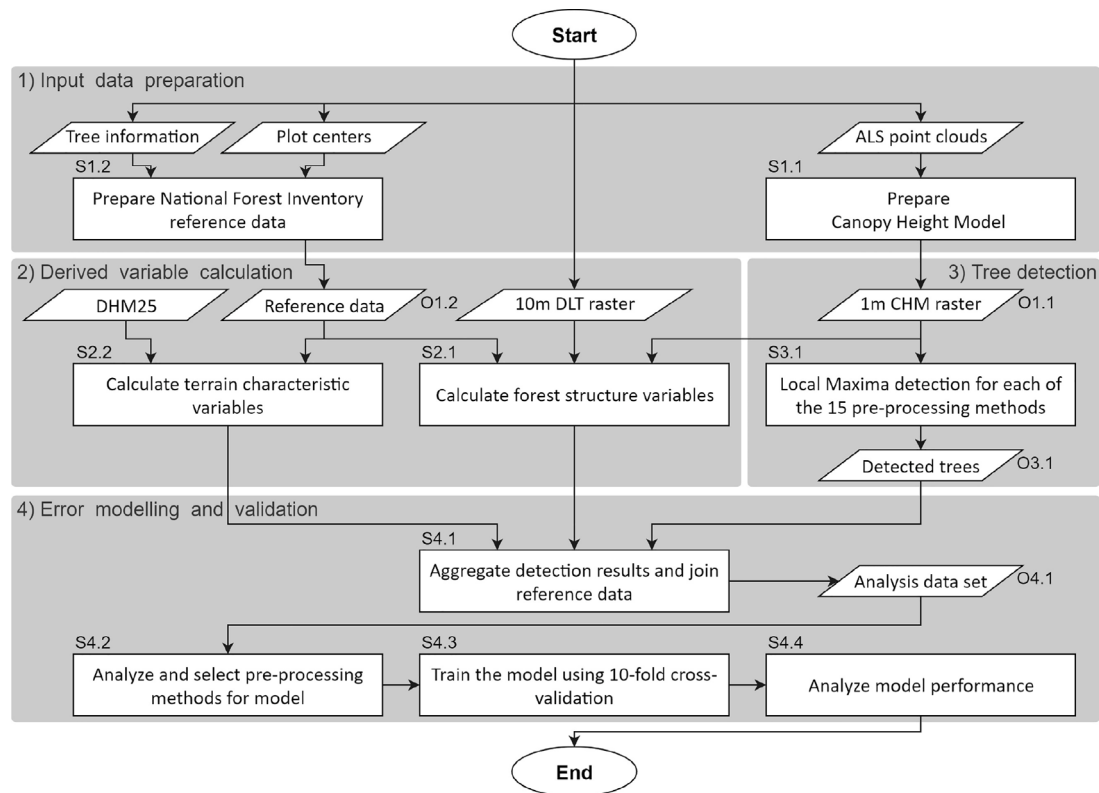
Fig. 3. Flow-chart of the methodology applied for this study. The boxes delineate separate stages.

cells). Starting with a window diameter of 3 cells, the diameter was expanded repeatedly until either a cell of the same or higher value was encountered or the maximum window diameter of 31 cells was reached. The final window diameter was an indicator for the dominance of the detected tree. In the detection algorithm, we included various options for pre-processing the CHM. These included resizing to variable cell sizes (using GDAL) and/or applying Gaussian filtering with variable kernel size and strength (using the scipy.signal.gaussian() function from the SciPy Python package). If a Gaussian filter was applied, the height of the detected trees was extracted from the unfiltered CHM.

Twelve filters and three filter combinations for CHM pre-processing were defined (see Table 3). The described LM algorithm was applied in combination with each of the filters (numbers 1 to 12). Each detection was executed over a circle with a 25 m radius from the plot center, whereby only detected trees within the outer plot circle of the NFI plot were retained. In addition, three combinations of multiple pre-processing filters (numbers 13 to 15 in Table 3) were tested. Each combination matched the result of the 1 m CHM detection with the results from two or more detections using the pre-processing filters. Thereby, only the trees detected in the 1 m CHM that matched a tree detected with at least one of the detections with pre-processing within a 1.5 m radius were retained, thereby reducing the trend to over-detect of the 1 m detection.

3.4. Error modeling and validation

3.4.1. Model for selecting pre-processing filters

Each pre-processing filter described in Table 3 was applied to all reference plots (step S3.1 in Fig. 3). Examples of the LM detection results of selected pre-processing filters are shown in the supplementary materials. The absolute number of trees in the plot, the stem count per ha, as well as the detection rate were calculated per plot and per pre-processing filter. The results were combined with the reference data and the forest structure variables (step S4.1 in Fig. 3). This combined

dataset was subsequently used to create a model that selects pre-processing filters, aiming to minimize the global error of the stem count per ha (detected stem count per ha vs. the inventory-based canopy stem count per ha - i.e., the number of trees in the upper canopy layer per ha). The modeling and analysis were performed in R (R Core Team, 2021).

Hybrid models, which combine two or more model types, are used in machine learning to improve overall model performance (Ardabili et al., 2019). For our hybrid model, we first fitted a model to predict the stem count error for each pre-processing filter. The errors were modeled in function of forest structure and terrain characteristic variables using multiple linear regression. Second, the rule-based part of the model selected the pre-processing filter whose predicted error value was closest to zero. If more than one method had the same minimal error, the filter with the lowest degree of filtering was selected. The model variables were selected based on variable importance analysis on regression models for the canopy stem count per ha, which were trained using a 10-fold cross-validation (James et al., 2021) with 3 repetitions. Variables with high importance in more than one pre-processing filter were selected for the final regression model (see Schaller and Dorren (2023) for details).

For the final validation, we configured the hybrid model with a suitable combination of pre-processing filters from Table 3 to reduce the overall detection errors of the LM algorithm (step S4.2 in Fig. 3). In an explorative analysis, the hybrid model exhibited the best balance between low overall detection errors and correct selection of pre-processing filters, using configurations with a combination of 7 to 12 pre-processing filters. Therefore, we selected a combination of 10 pre-processing filters (numbers 1, 2, 3, 7, 8, 9, 10, 11, 12, and 15 in Table 3) from a larger set of combinations with similar detection errors and accuracy to configure the hybrid model.

3.4.2. Model performance assessment

Since our study focused on improving the overall detection result based on forest structure, the performance assessment for our model

Table 2
Forest structure and terrain characteristic variables for model input calculated on the 25 m cell size raster.

Variable name	Description	Reference
Forest structure variables		
h_{dom}	Dominant height = 80th percentile of the cell values	
dg	Degree of cover (dg) as percentage of cells with $h < (2/3 * h_{dom})$	Rosset (2021)
dg_{no_layer}	dg no layer ($h < 0.4m$)	
dg_{us}	dg lower layer ($0.4m \le h \le (1/3 * h_{dom})$)	
dg_{ms}	dg middle layer ($(1/3 * h_{dom}) < h \le (2/3 * h_{dom})$)	
dg_{os}	dg upper layer ($(2/3 * h_{dom}) < h \le h_{dom}$)	
dg_{ueb}	dg protrusions ($h_{dom} < h$)	
mg	Dominant leaf calculated as mean of the touched DLT cells	
CHM characteristic variables		
TPI	Topographic Position Index (minimum, maximum, mean, median, standard deviation)	Wilson et al. (2007)
TRI	Terrain Roughness Index (minimum, maximum, mean, median, standard deviation)	
Terrain characteristic variables (nearest neighbor)		
z	Altitude in m above sea level	
Slope	Slope in degrees	
Aspect	Aspect in degrees	
Aspect northness Aspect eastness	Cosine(aspect) * sine(slope) Sine(aspect) * sine(slope)	Fassnacht et al. (2003)

Table 3
Tested filter methods for CHM pre-processing.

Nr.		Filter name	Description
1	[a]	1 m	1 by 1 m unresized cell size without filter
2	[a]	1.5 m	Bilinear resizing to 1.5 by 1.5 m cell size without filter
3	[a]	2 m	Bilinear resizing to 2 by 2 m cell size without filter
4		1 m, std 1, size 3	1 by 1 m unresized cell size gaussian filter using a standard deviation of sigma = 1 and window size of 3, 5, and 7 cells
5		1 m, std 1, size 5	
6		1 m, std 1, size 7	
7	[a]	1 m, std 2, size 3	1 by 1 m unresized cell size gaussian filter using a standard deviation of sigma = 2 and window size of 3, 5, and 7 cells
8	[a]	1 m, std 2, size 5	
9	[a]	1 m, std 2, size 7	
10	[a]	1 m, std 3, size 3	1 by 1 m unresized cell size gaussian filter using a standard deviation of sigma = 3 and window size of 3, 5, and 7 cells
11	[a]	1 m, std 3, size 5	
12	[a]	1 m, std 3, size 7	
13		Combined 1 m/1.5 m/1 m, std2, d3	Combination of the "1 m" base detection with the "1.5 m" and "1 m, std 2, size 3" detection results
14		Combined 1 m/2 m/1 m, std2, d5	Combination of the "1 m" base detection with the "2 m" and "1 m, std 2, size 5" detection results
15	[a]	Combined 1 m/1.5 m/1 m, std1, d3/1 m, std2, d3/1 m, std3, d3	Combination of the "1 m" base detection with the "1.5 m", "1 m, std 1, size 3", "1 m, std 2, size 3", and "1 m, std 3, size 3" detection results

[a] Part of final hybrid model configuration.

was carried out at the plot level (step S4.4 in Fig. 3). We used the mean absolute error (MAE) of the detected stem count per ha versus the inventory-based canopy stem count per ha as the primary performance assessment measure, which was calculated as:

$$MAE_N = \frac{1}{n_{plots}} \Sigma_{i=1}^{n_{plots}} \left| N_{model\_i} - N_{actual\_i} \right| \tag{1}$$

where:

MAE_N: Mean Absolute Error of the stem count per ha

N_{actual_i}: Canopy stem count per ha (i.e., trees in the upper canopy layer per ha) in plot i according to NFI

N_{model_i}: Stem count per ha for the trees detected in plot i according to the model

n_{plots}: Total number of reference plots

Additionally, the median of the detected stem count normalized by the inventory-based canopy stem count was calculated as a relative performance measure, following:

$$MedAE_{N\_norm} = Median\left(\frac{|N_{model\_i} - N_{actual\_i}|}{N_{actual\_i}}\right) \tag{2}$$

where:

$MedAE_{N\_norm}$: Median normalized Absolute Error of the stem count per ha

As secondary performance criteria the mean and median detection rates (dr_{mean}, resp. dr_{median}) were calculated as measures for under-/over-detection, following:

$$dr_{mean} = \frac{1}{n_{plots}} \Sigma_{i=1}^{n_{plots}} \left(\frac{N_{model\_i}}{N_{actual\_i}}\right) \tag{3}$$

$$dr_{median} = Median\left(\frac{N_{model\_i}}{N_{actual\_i}}\right) \tag{4}$$

The input dataset was randomly partitioned into calibration (80% of the data) and validation (20%) data. A 10-fold cross-validation was performed to calibrate the model, which was subsequently validated (step S4.3 in Fig. 3). For model comparison, the performance measures were also calculated for the Baseline detection using the unfiltered 1 m cell size CHM (hereafter referred to as Baseline) and a well performing method based on (Eysn et al., 2015, hereafter referred to as Eysn). This method combines a closing filter (disk size=1) and Gauss filter (sigma = 0.5 on a 3 by 3 neighborhood). The calibration and validation procedure was performed on the complete dataset (i.e. all plots) as well as on two subsets. Since higher point densities may improve detection performance (Sparks et al., 2022), subset A only included plots where the ALS acquisition was performed in 2010 or later to ensure high point densities (c.f. Table 1). Subset B further reduced subset A by the additional requirement that the difference between the ALS acquisition year and the year of the field inventory was max. 6 years. The 6-year limit was chosen because it covers a time-span similar to one NFI recording period while retaining sufficient reference plots. While this limits the potential differences between ALS acquisition and the field inventory, larger changes (e.g. through harvesting or storm damage) are still possible.

For county-wide applications, the model from the fold with the smallest MAE_N was selected. The performance measures were calculated based on an application of the selected model to the three validation datasets. The performance measures included the detection error MAE_N, the median normalized absolute error $MedAE_{N\_norm}$, the mean detection rate dr_{mean}, and the median detection rate dr_{median}. These performance measures were calculated for the entire validation data as well as differentiated by mixing degree, the degree of cover, and the dominant stand height. For the mixing degree, we differentiated between coniferous-dominated plots (proportion of coniferous trees (NH) > 70%), for mixed plots (NH between 30% and 70%) as well as for broadleaved-dominated plots (NH ≤ 30%). For the degree of cover (DG), we differentiated between dense (DG > 80%) and open (DG ≤80%) plots, and for the h_{dom} we differentiated between high

Table 4

Summary of the model performance of the calibrated hybrid models along with corresponding performance values for the Eysn and Baseline detections. The values represent mean values of the results from applying the models from all 10 calibration folds to the validation plots of the respective datasets: (1) all reference plots; (2) subset A, excluding all plots with ALS acquisition year before 2010; (3) subset B, excluding all plots with ALS acquisition year before 2010 and a difference between ALS acquisition and field inventory of max. 6 years.

Dataset	n_{plots}	Method	MAE_N	$MedAE_{N\_norm}$	dr_{mean}	dr_{median}
(1) All plots validation	1048	Model	64	0.33	1.31	1.00
		Eysn	69	0.33	1.35	0.90
		Baseline	167	1.00	3.05	2.00
(2) Subset A validation	757	Model	66	0.33	1.29	1.00
		Eysn	75	0.36	1.40	0.90
		Baseline	172	0.92	3.10	1.92
(3) Subset B validation	532	Model	61	0.33	1.27	1.00
		Eysn	73	0.40	1.51	1.00
		Baseline	174	1.00	3.21	2.00

($h_{dom} > 22$ m) and low ($h_{dom} \leq 22$ m) dominant height within the plot. Of the 5254 reference plots, 46% are coniferous-, 35% broadleaved-dominated, and 19% mixed; 36% are dense and 45% show a low dominant height.

4. Results

Table 4 shows the summarized results from the validation of the hybrid model calibrated on different subsets of the NFI reference plots along with the corresponding values for the Baseline 1 m and Eysn detections. For the validation of the dataset with all reference plots, the MAE_N value of 64 stems per ha of the model is less than half the value compared to the MAE_N of 167 stems per ha of the Baseline and 69 trees for the Eysn detection (with an average inventory-based canopy stem count of 170 stems per ha). The mean detection rate dr_{mean} is similarly reduced from 3.05 to 1.31, which shows that there still is over-detection. For the subsets A and B, the performance measure values and their changes are comparable to the dataset with all reference plots. The values and changes of the performance measures from the calibration of the model are also comparable to the corresponding validation values. All results are presented in the notebook accompanying this publication (Schaller and Dorren, 2023).

The model of subset B resulted in the smallest MAE_N and was therefore selected for the country-wide application. For this subset, the performance measure values of the model showed only small variations when differentiating between the plots by mixing degrees (Table 5). However, the Baseline detection values showed clear differences. The Eysn detection also showed clear differences, albeit on a lower scale. The values of the mixed plots were generally comparable to the values of all plots. Broadleaved-dominated plots show higher MAE_N, and coniferous-dominated plots show significantly lower MAE_N values.

The model also showed similar performance for both classes when differentiating the plots by dominant height (h_{dom}). The MAE_N for the model is similar for both classes while the Baseline and Eysn MAE_N are slightly better for plots with the higher h_{dom}. The $MedAE_{N\_norm}$ and the dr_{mean} of the model are, however, noticeably higher for the group with a lower h_{dom} when compared to the other group. Similarly, the Baseline and Eysn $MedAE_{N\_norm}$ and dr_{mean} are higher in the group with the lower h_{dom}.

When differentiating between plots with high and low degrees of cover, the performance differs noticeably. The MAE_N of 50 stems per ha for plots with low degrees of cover is clearly lower and the MAE_N of 76 stems per ha for high degrees of cover is clearly higher than the 61 stems per ha for all plots. In comparison, the MAE_N for the Baseline and Eysn detections show similar trends, but the values are clearly higher than the model.

Fig. 4 shows the distributions of the stem count per ha for the inventory data, the combination of different pre-processing filters based

on the model, the 1 m Baseline detection, and the Eysn detection with the corresponding detection errors. The actual values show the inventory-based canopy stem count per ha. The distribution of the stem count based on the predictions of our model and the Eysn detection are clearly closer to the actual distribution than the Baseline detection, whose mean value is about 1.5 times as high. The distribution of the detection errors of our model is centered around the median of 0 stems per ha, while the Baseline detection shows higher values with a median of 155 stems per ha, reflecting the stronger trend towards over-detection. The error of the Eysn detection is close to our model but shows a slightly lower mean value.

Fig. 5 shows scatter diagrams of the actual inventory-based canopy stem counts per ha compared to the different detection methods. The trend to over-detect when using the unfiltered CHM is clearly visible in diagram (c), as many points are above the diagonal (Fig. 5, upper right). The scatter diagram of the model in diagram (a) is closer to the diagonal (Fig. 5, lower right), but still exhibits a large variance. The values of the Eysn method in (b) are also closer to the diagonal (Fig. 5, upper left), but show a stronger trend to under-detection.

5. Discussion

5.1. Detection performance

In this study, we aimed to improve a CHM-based LM tree detection method for a country-wide application using statistical modeling and prior knowledge about forest structure. The results showed that CHM-based LM methods for individual tree detection can be improved by considering prior knowledge about forest structure. While others have used prior knowledge (e.g. Heinzel et al., 2011; Ene et al., 2012; Zhen et al., 2015; Stereńczak et al., 2020) to adjust CHM filtering, the hybrid model combines statistical error models based on an array of forest structure variables and a rule-based model. Our model resulted in clear improvement of the detection errors and mostly constant performance over forest structures with different dominant height (h_{dom}), degree of cover, and dominant leaf type (DLT). Using the hybrid model for CHM pre-processing in a LM algorithm reduced the MAE of the detection by at least 50% compared to the detection MAE of a Baseline LM detection without CHM pre-processing. Compared to the Eysn method, our model still performs slightly better. Furthermore, the Eysn method shows a tendency towards more under-detection and higher performance differences between different h_{dom}, degree of cover, and DLT.

Other studies using LM-based detection (e.g. Popescu et al., 2003; Kaartinen et al., 2012; Eysn et al., 2015) typically showed an improvement of the detection accuracy by 20%–30% for single-layered coniferous-dominated plots when compared to mixed or broadleaved-dominated plots. In our study, the Baseline detection on the unfiltered CHM and the Eysn method showed similar trends and performed better for coniferous-dominated plots than for mixed or broadleaved-dominated plots when differentiating the plots according to the DLT. The performance of our hybrid model, however, showed only small differences between the DLT classes and only slightly better detection for coniferous-dominated plots compared to mixed and broadleaved-dominated plots. A detailed analysis of the detection errors in comparison to the DLT did show a decrease of the median error of the model with increasing coniferous proportion from 38% for pure broadleaved plots to 25% for pure coniferous plots. The results have shown that the hybrid model could improve LM-based individual tree detection in coniferous and broadleaved plots with a significant improvement in broadleaved-dominated plots.

Despite clear improvements in detection performance using our model, there was still a trend towards over-detection. The values of the stem count MAE_N between 61 and 66 stems per ha of the model seem to be relatively high. However, the detection rate indicates an average over-detection of only 27% to 31%. This is partially supported by the median of the normalized absolute error $MedAE_{N\_norm}$ values of around

Table 5

Detailed performance results for the application of the model to plots of subset B along with corresponding performance values for the Eysn and Baseline detections. Groups: (a) All plots; (b) DLT broadleaved-dominated plots (proportion of coniferous trees ≤30%); (c) DLT mixed plots (proportion of coniferous trees between 30% and 70%); (d) DLT coniferous-dominated plots (proportion of coniferous trees according to the DLT raster >70%); (e) DG ≤ 80%, (f) DG > 80%; (g) h_{dom} ≤ 22 m; (h) h_{dom} > 22 m.

| Grouping	Group	n_{plots}	Method	MAE_N	$MedAE_{N\_norm}$	dr_{mean}	dr_{median}
All plots validation	(a) All plots	532	Model	61	0.33	1.28	1.00
			Eysn	73	0.40	1.51	1.00
			Baseline	174	1.00	3.21	2.00
Dominant leaf type validation	(b) Broadleaved	220	Model	64	0.35	1.36	1.00
			Eysn	76	0.39	1.72	1.00
			Baseline	233	1.50	3.98	2.50
	(c) Mixed	108	Model	65	0.33	1.24	0.96
			Eysn	81	0.40	1.62	0.91
			Baseline	175	0.92	3.43	1.92
	(d) Coniferous	204	Model	55	0.29	1.23	1.00
			Eysn	67	0.40	1.24	0.89
			Baseline	109	0.58	2.26	1.57
Degree of cover validation	(e) DC ≤ 80%	309	Model	50	0.37	1.40	1.00
			Eysn	62	0.44	1.67	1.20
			Baseline	155	1.30	3.52	2.30
	(f) DC > 80%	223	Model	76	0.30	1.12	0.88
			Eysn	89	0.31	1.29	0.83
			Baseline	199	0.82	2.77	1.82
Dominant height validation	(f) h_{dom} ≤ 22 m	206	Model	63	0.39	1.55	1.00
			Eysn	83	0.50	2.19	1.27
			Baseline	193	1.50	4.40	2.50
	(h) h_{dom} > 22 m	326	Model	60	0.29	1.11	1.00
			Eysn	68	0.33	1.09	0.86
			Baseline	161	0.85	2.46	1.85
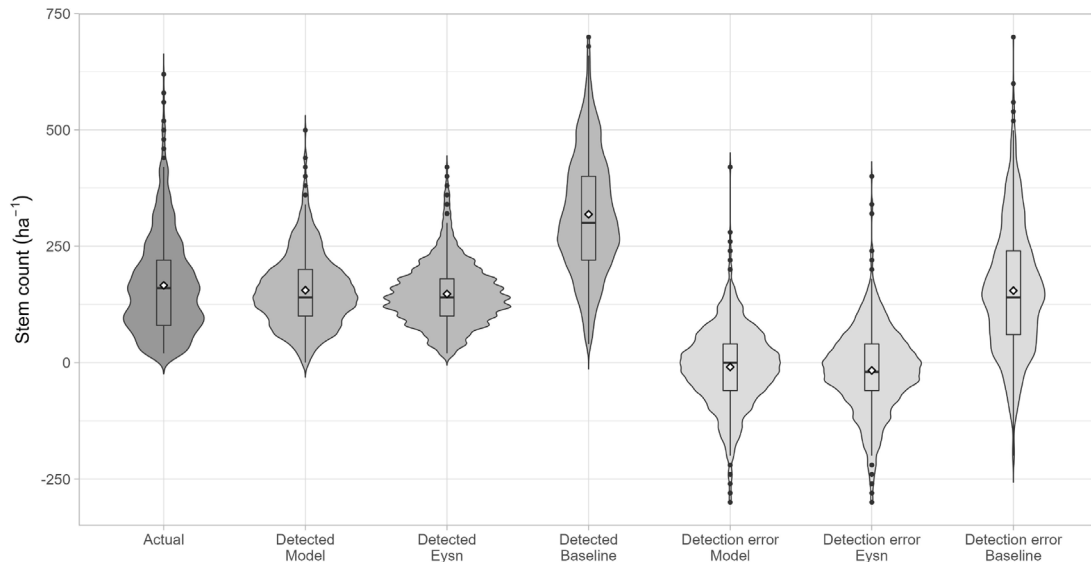
Fig. 4. Violin plots of the canopy stem count distributions per ha. Actual: calculated from the reference inventory plots; Detected model: count of the detected stems using the calibrated model (R2: 0.35, median bias: 19.99); Detected Eysn: count of the detected stems using the Eysn method (R2: 0.25, median bias: 19.99); Detected Baseline: count of the detected stems using the Baseline method (R2: 0.13, median bias: −139.90); Detection error model: distribution of errors between the detection using the calibrated model and the reference data; Detection error Eysn: distribution of errors for the Eysn method; Detection error Baseline: distribution of errors for the Baseline detection method. The mean values of all distributions are shown as open white dots within the box plots. Outliers are shown as small black dots. A few outliers lie outside the plotted stem count range.

0.33. This over-detection is put into perspective by the relatively large value range with clear outliers and the median detection rate of around 1 from the detailed application of the model over all plots. These results and the trends in model performance can be mostly explained by the reference data used in the study and the aims of the model.

Firstly, the time difference between the acquisition of the Airborne Laser Scanning (ALS) data and the field measurements for the NFI of Switzerland influenced the result. A longer time difference between ALS acquisition and field measurements increases the probability of forest cover changes in the plots, for example, due to logging or storm damage, which leads to differences between detection and reference data. While a detailed analysis of the influence of the point density on detection results is outside the scope of this study, the exclusion of plots with lower point densities seems to have little effect on the performance. Whereas the dr_{mean} slightly improves, the MAE_N slightly increases. Although some studies reported a positive effect of higher point densities on CHM based tree detection (Wallace et al., 2014; Sparks et al., 2022) our results are more in line with studies stating that point density has no significant effect (Kaartinen et al., 2012; Ruiz et al., 2014). On the other hand, there is a slight increase in model performance when additionally excluding plots with a difference
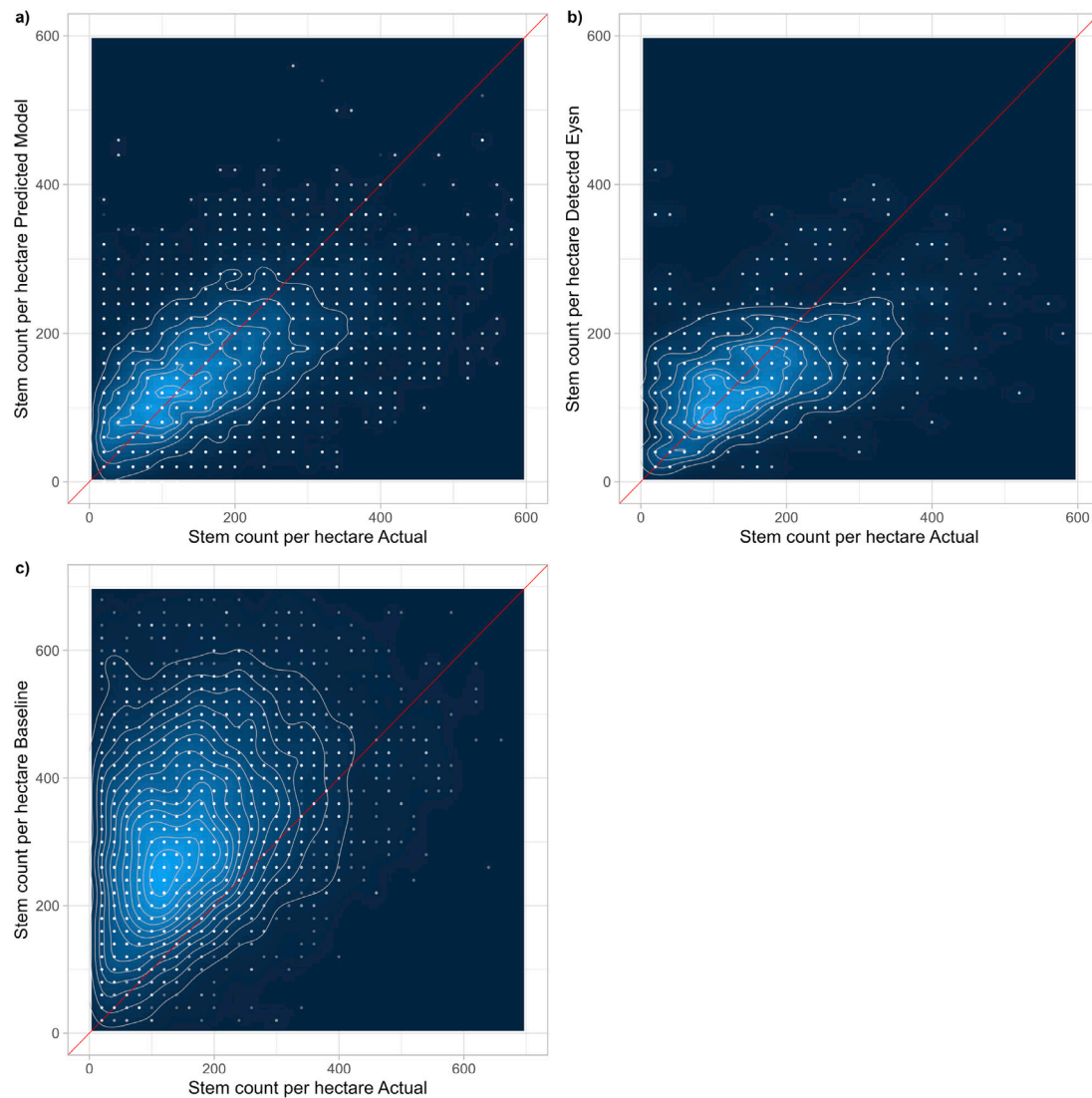
Fig. 5. Scatter diagrams of (a) the actual canopy stem counts per ha vs. predicted stem count per ha for the predictions from applying the individual models from the cross-validation (b) the actual vs. detected stem count from the Eysn detection, and (c) the actual vs. detected stem counts per ha from the Baseline detection. The diagrams have a 2D kernel density plot including contours in the background as well as the identity line in red. (For interpretation of the references to color in this figure legend, the reader is referred to the web version of this article.)

of more than 6 years between ALS acquisition and NFI measurements. Other studies similarly emphasized the importance of input data characteristics (Wallace et al., 2014; Eysn et al., 2015; Price et al., 2020).

Secondly, part of the over-detection also results from the fact that only the trees in the emergent and canopy layer, which are potentially detectable by LM, were used as references. Using all inventory trees would have resulted in higher absolute stem count errors and a general trend towards under-detection. Furthermore, in the outer circle of the inventory plots, only trees with a diameter of at least 36 cm were measured, thus potentially excluding detectable trees from the inventory.

Lastly, our model emphasizes an average improvement of the detection error over a wide range of forest structures. Other studies reported clearer improvements from CHM filtering. However, even in larger comparative studies, such as Vauhkonen et al. (2012) with 77 plots over five locations or Eysn et al. (2015) with 18 plots over eight locations, the reference data and the variety in the forest structure were limited. In this study, on the other hand, the wide geographic distribution of the NFI reference plots across Switzerland resulted in a comparatively large number of reference plots and higher variability

in forest structures. Therefore, our model needs to generalize a wide variety of forest structures and consequently the applied pre-processing filters may not be optimal for all plots. Investigating plots with high detection errors showed that they can be found in almost all forest types, but outliers seem to occur more frequently in plots with low dominant stand heights.

5.2. Hybrid model robustness

Our hybrid model for selecting pre-processing filters showed a stable performance and similar performance values for both the calibration and validation data. This suggests a robust model with a low degree of over-fitting. Based on the underlying linear regression models, the classical forest structure variables like the dominant height, DLT, and different degrees of cover have shown to be of high importance for most of the pre-processing filters. Additionally, the northness and the altitude above sea level derived from the digital height model were important in most cases. Several of the model variables are similar to variables used by (e.g. Koch et al., 2006; Heinzel et al., 2011; Ene et al., 2012; Zhen et al., 2015).
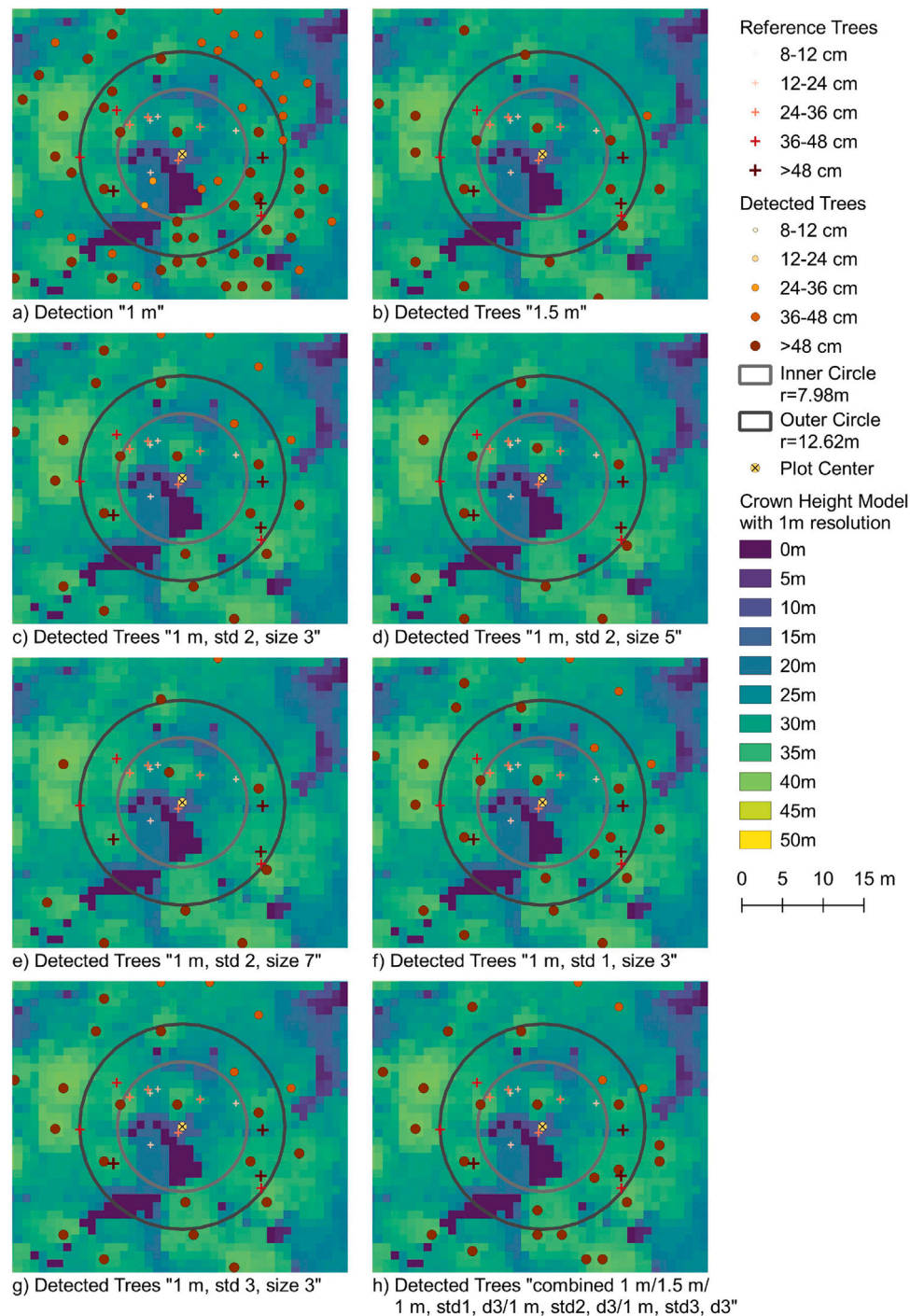
Fig. A.6. An example of the LM detection results using different pre-processing filters. The displayed NFI reference plot (shown by the two circles) is situated in a forest with approx. 60% coniferous trees.

Our model exhibited very similar performance for a wide range of method combinations during the exploration of different pre-processing filter combinations. Given the large number of different reference plots and the variability in the input data, we consider the observed model performance and the obtained detection results to be valuable complementary datasets. The country-wide application of the hybrid model took 16 days on a Dell PowerEdge R640 server with two Intel Xeon Gold 6152 CPU (total 44 cores) and 448 GB memory. The resulting data can now be used in a range of modeling applications that require data on stem counts and forest structure over large areas, such as natural hazard process models that simulate interactions with single trees or forest growth models.

6. Conclusion

We conclude that the hybrid model improved the detection performance by consistently reducing the detection errors by at least 50%, with a slight trend towards over-detection. Thereby, the model performed equally well for different dominant leaf types (broadleaved-dominated, mixed, coniferous-dominated) and for different degrees of cover. We attribute the stable performance to the good quality of the calibration data, that comprised a large number of reference plots with a wide variety of forest structures. We consider the hybrid model to be suitable for applications that require data on forest structure

or individual tree positions and heights over large areas. Especially for areas with diverse forest structures, the application of our model provides an overall improvement of detection results compared to a simple detection without CHM pre-processing.

CRediT authorship contribution statement

Christoph Schaller: Conceptualization, Methodology, Software, Validation, Formal analysis, Investigation, Resources, Data curation, Writing – original draft, Writing – review & editing, Visualization. **Christian Ginzler:** Data curation, Writing – original draft, Writing – review & editing. **Emiel van Loon:** Methodology, Writing – review & editing, Supervision. **Christine Moos:** Methodology, Writing – review & editing. **Arie C. Seijmonsbergen:** Writing – review & editing, Supervision. **Luuk Dorren:** Conceptualization, Methodology, Software, Writing – original draft, Writing – review & editing, Supervision, Project administration, Funding acquisition.

Declaration of competing interest

The authors declare that they have no known competing financial interests or personal relationships that could have appeared to influence the work reported in this paper.

Data availability

The authors do not have permission to share data. A repository containing the code used in this sudy can be found in the references.

Appendix. Supplementary material

See Fig. A.6.

References

Ardabili, S., Mosavi, A., Várkonyi-Kóczy, A.R., 2019. Advances in machine learning modeling reviewing hybrid and ensemble methods. In: Int. Conf. Global Res. Educ.. Springer, pp. 215–227. http://dx.doi.org/10.1007/978-3-030-36841-8_21.

Brändli, U., Abegg, M., Allgaier Leuch, B., 2020. Schweizerisches Landesforstinventar. Ergebnisse der vierten Erhebung 2009–2017. Eidg. Forschungsanstalt für Wald, Schnee und Landschaft WSL, Birmensdorf, und Bern, Bundesamt für Umwelt, Bern.

Breidenbach, J., Astrup, R., 2014. The semi-individual tree crown approach. In: Forestry Applications of Airborne Laser Scanning. Springer, pp. 113–133. http://dx.doi.org/10.1007/978-94-017-8663-8_6.

Ene, L., Næsset, E., Gobakken, T., 2012. Single tree detection in heterogeneous boreal forests using airborne laser scanning and area-based stem number estimates. Int. J. Remote Sens. 33 (16), 5171–5193. http://dx.doi.org/10.1080/01431161.2012.657363.

Eysn, L., Hollaus, M., Lindberg, E., Berger, F., Monnet, J.-M., Dalponte, M., Kobal, M., Pellegrini, M., Lingua, E., Mongus, D., Pfeifer, N., 2015. A benchmark of lidar-based single tree detection methods using heterogeneous forest data from the alpine space. Forests 6 (12), 1721–1747. http://dx.doi.org/10.3390/f6051721.

Fassnacht, S.R., Dressler, K.A., Bales, R.C., 2003. Snow water equivalent interpolation for the Colorado River Basin from snow telemetry (SNOTEL) data. Water Resour. Res. 39 (8), http://dx.doi.org/10.1029/2002WR001512.

Fischer, C., Traub, B., 2019. Swiss National Forest Inventory – Methods and Models of the Fourth Assessment, Vol. 35. Springer International Publishing, http://dx.doi.org/10.1007/978-3-030-19293-8.

GDAL/OGR contributors, 2021. GDAL/OGR Geospatial Data Abstraction software library. https://gdal.org (accessed: 10 July 2021).

Harrison, P.A., Vandewalle, M., Sykes, M.T., Berry, P.M., Bugter, R., de Bello, F., Feld, C.K., Grandin, U., Harrington, R., Haslett, J.R., Jongman, R.H.G., Luck, G.W., da Silva, P.M., Moora, M., Settele, J., Sousa, J.P., Zobel, M., 2010. Identifying and prioritising services in European terrestrial and freshwater ecosystems. Biodivers. Conserv. 19 (10), 2791–2821. http://dx.doi.org/10.1007/s10531-010-9789-x.

Heinzel, J.N., Weinacker, H., Koch, B., 2011. Prior-knowledge-based single-tree extraction. Int. J. Remote Sens. 32 (17), 4999–5020. http://dx.doi.org/10.1080/01431161.2010.494633.

Hui, Z., Cheng, P., Yang, B., Zhou, G., 2022. Multi-level self-adaptive individual tree detection for coniferous forest using airborne LiDAR. Int. J. Appl. Earth Observ. Geoinf. 114, 103028. http://dx.doi.org/10.1016/j.jag.2022.103028.

Hyyppä, J., Hyyppä, H., Inkinen, M., Engdahl, M., Linko, S., Zhu, Y.-H., 2000. Accuracy comparison of various remote sensing data sources in the retrieval of forest stand attributes. Forest Ecol. Manag. 128 (1–2), 109–120. http://dx.doi.org/10.1016/S0378-1127(99)00278-9.

Hyyppä, J., Hyyppä, H., Leckie, D., Gougeon, F., Yu, X., Maltamo, M., 2008. Review of methods of small–footprint airborne laser scanning for extracting forest inventory data in boreal forests. Int. J. Remote Sens. 29 (5), 1339–1366. http://dx.doi.org/10.1080/01431160701736489.

James, G., Witten, D., Hastie, T., Tibshirani, R., 2021. An Introduction to Statistical Learning. Springer US, http://dx.doi.org/10.1007/978-1-0716-1418-1.

Kaartinen, H., Hyyppä, J., Yu, X., Vastaranta, M., Hyyppä, H., Kukko, A., Holopainen, M., Heipke, C., Hirschmugl, M., Morsdorf, F., Næsset, E., Pitkänen, J., Popescu, S., Solberg, S., Wolf, B.M., Wu, J.-C., 2012. An international comparison of individual tree detection and extraction using airborne laser scanning. Remote Sens. 4 (4), 950–974. http://dx.doi.org/10.3390/rs4040950.

Kangas, A., Jeffrey, H.G., Scott, C.T., 2006. Introduction (chapter 1). In: Kangas, A., Maltamo, M. (Eds.), Forest inventory, methodology and applications. In: Managing forest ecosystems, vol. 10, Springer, Dordrecht, Netherlands, pp. 3–11. http://dx.doi.org/10.1007/1-4020-4381-3_1.

Koch, B., Heyder, U., Weinacker, H., 2006. Detection of individual tree crowns in airborne lidar data. Photogramm. Eng. Remote Sens. 72 (4), 357–363. http://dx.doi.org/10.14358/PERS.72.4.357.

Koch, B., Kattenborn, T., Straub, C., Vauhkonen, J., 2014. Segmentation of forest to tree objects. In: Forestry Applications of Airborne Laser Scanning. Springer, pp. 89–112. http://dx.doi.org/10.1007/978-94-017-8663-8_5.

Kolendo, u., Kozniewski, M., Ksepko, M., Chmur, S., Neroj, B., 2021. Parameterization of the individual tree detection method using large dataset from ground sample plots and airborne laser scanning for stands inventory in coniferous forest. Remote Sens. 13 (14), 2753. http://dx.doi.org/10.3390/rs13142753, PII: rs13142753.

Kukkonen, M., Maltamo, M., Korhonen, L., Packalen, P., 2021. Fusion of crown and trunk detections from airborne UAS based laser scanning for small area forest inventories. Int. J. Appl. Earth Observ. Geoinf. 100, 102327. http://dx.doi.org/10.1016/j.jag.2021.102327.

Luo, Z., Zhang, Z., Li, W., Chen, Y., Wang, C., Nurunnabi, A.A.M., Li, J., 2022. Detection of individual trees in UAV LiDAR point clouds using a deep learning framework based on multichannel representation. IEEE Trans. Geosci. Remote Sens. 60, 1–15. http://dx.doi.org/10.1109/TGRS.2021.3130725.

Michałowska, M., Rapiński, J., 2021. A review of tree species classification based on airborne LiDAR data and applied classifiers. Remote Sens. 13 (3), 353. http://dx.doi.org/10.3390/rs13030353.

Mielcarek, M., Stereńczak, K., Khosravipour, A., 2018. Testing and evaluating different LiDAR-derived canopy height model generation methods for tree height estimation. Int. J. Appl. Earth Observ. Geoinf. 71, 132–143. http://dx.doi.org/10.1016/j.jag.2018.05.002.

Osco, L.P., Junior, J.M., Ramos, A.P.M., de Castro Jorge, L.A., Fatholahi, S.N., de Andrade Silva, J., Matsubara, E.T., Pistori, H., Gonçalves, W.N., Li, J., 2021. A review on deep learning in UAV remote sensing. Int. J. Appl. Earth Observ. Geoinf. 102, 102456. http://dx.doi.org/10.1016/j.jag.2021.102456.

Pohjanmies, T., Triviño, M., Le Tortorec, E., Mazziotta, A., Snäll, T., Mönkkönen, M., 2017. Impacts of forestry on boreal forests: An ecosystem services perspective. Ambio 46 (7), 743–755. http://dx.doi.org/10.1007/s13280-017-0919-5.

Popescu, S.C., Wynne, R.H., Nelson, R.F., 2003. Measuring individual tree crown diameter with lidar and assessing its influence on estimating forest volume and biomass. Can. J. Remote Sens. 29 (5), 564–577. http://dx.doi.org/10.5589/m03-027.

Price, B., Waser, L.T., Wang, Z., Marty, M., Ginzler, C., Zellweger, F., 2020. Predicting biomass dynamics at the national extent from digital aerial photogrammetry. Int. J. Appl. Earth Observ. Geoinf. 90, 102116. http://dx.doi.org/10.1016/j.jag.2020.102116.

R Core Team, 2021. R: A language and environment for statistical computing. https://www.R-project.org/ (accessed: 10 July 2021).

Rigling, A., Schaffer, H.P., 2015. Forest report 2015. condition and use of swiss forests. In: Federal Office for the Environment, Bern. Swiss Federal Institute WSL, Birmensdorf, p. 144.

Rosset, C., 2021. La valeur ajoutée de la digitalisation: être plusinformé, connecté et agile. Schweiz. Z. Forstwes. 172 (4), 198–204. http://dx.doi.org/10.3188/szf.2021.0198.

Ruiz, L.A., Hermosilla, T., Mauro, F., Godino, M., 2014. Analysis of the influence of plot size and lidar density on forest structure attribute estimates. Forests 5 (5), 936–951. http://dx.doi.org/10.3390/f5050936.

Schaller, C., Contributors, 2022. pyFINT: Python implementation of FINT. http://dx.doi.org/10.5281/zenodo.6543289.

Schaller, C., Dorren, L., 2023. HAFL-WWI/FINTCH-publication-code: "Improving country-wide individual tree detection using local maxima methods based on statistically modeled forest structure information (2023)" v0.2.2. http://dx.doi.org/10.5281/zenodo.8260871.

Sparks, A.M., Corrao, M.V., Smith, A.M.S., 2022. Cross-comparison of individual tree detection methods using low and high pulse density airborne laser scanning data. Remote Sens. 14 (14), http://dx.doi.org/10.3390/rs14143480.

Stereńczak, K., Kraszewski, B., Mielcarek, M., Piasecka, Ż., Lisiewicz, M., Heurich, M., 2020. Mapping individual trees with airborne laser scanning data in an European lowland forest using a self-calibration algorithm. Int. J. Appl. Earth Observ. Geoinf. 93, 102191. http://dx.doi.org/10.1016/j.jag.2020.102191.

Swisstopo, 2021a. DHM25 - The digital height model of Switzerland. https://www.swisstopo.admin.ch/en/geodata/height/dhm25.html (accessed: 10 July 2021).

Swisstopo, 2021b. swissALTI3D. https://www.swisstopo.admin.ch/en/geodata/height/alti3d.html (accessed: 10 July 2021).

Swisstopo, 2021c. swissSURFACE3D. https://www.swisstopo.admin.ch/en/geodata/height/surface3d.html (accessed: 10 July 2021).

van Rossum, G., Drake, F.L., 2009. Python 3 Reference Manual. CreateSpace.

Vandendaele, B., Fournier, R.A., Vepakomma, U., Pelletier, G., Lejeune, P., Martin-Ducup, O., 2021. Estimation of northern hardwood forest inventory attributes using UAV laser scanning (ULS): Transferability of laser scanning methods and comparison of automated approaches at the tree- and stand-level. Remote Sens. 13 (14), 2796. http://dx.doi.org/10.3390/rs13142796.

Vauhkonen, J., Ene, L., Gupta, S., Heinzel, J., Holmgren, J., Pitkänen, J., Solberg, S., Wang, Y., Weinacker, H., Hauglin, K.M., Lien, V., Packalén, P., Gobakken, T., Koch, B., Næsset, E., Tokola, T., Maltamo, M., 2012. Comparative testing of single-tree detection algorithms under different types of forest 85. pp. 27–40.

Wallace, L., Lucieer, A., Malenovský, Z., Turner, D., Vopěnka, P., 2016. Assessment of forest structure using two UAV techniques: A comparison of airborne laser scanning and structure from motion (SfM) point clouds. Forests 7 (12), 62. http://dx.doi.org/10.3390/f7030062.

Wallace, L., Lucieer, A., Watson, C.S., 2014. Evaluating tree detection and segmentation routines on very high resolution UAV LiDAR data. IEEE Trans. Geosci. Remote Sens. 52 (12), 7619–7628. http://dx.doi.org/10.1109/TGRS.2014.2315649.

Waser, L., Ginzler, C., 2018. Forest type NFI. http://dx.doi.org/10.16904/1000001.7.

Waser, L.T., Rüetschi, M., Psomas, A., Small, D., Rehush, N., 2021. Mapping dominant leaf type based on combined Sentinel-1/-2 data – Challenges for mountainous countries. ISPRS J. Photogramm. Remote Sens. 180, 209–226. http://dx.doi.org/10.1016/j.isprsjprs.2021.08.017.

Williams, J., Schonlieb, C.-B., Swinfield, T., Lee, J., Cai, X., Qie, L., Coomes, D.A., 2020. 3D segmentation of trees through a flexible multiclass graph cut algorithm. IEEE Trans. Geosci. Remote Sens. 58 (2), 754–776. http://dx.doi.org/10.1109/TGRS.2019.2940146.

Wilson, M.F.J., O'Connell, B., Brown, C., Guinan, J.C., Grehan, A.J., 2007. Multiscale terrain analysis of multibeam bathymetry data for habitat mapping on the continental slope. Mar. Geod. 30 (1–2), 3–35. http://dx.doi.org/10.1080/01490410701295962.

Xu, X., Zhou, Z., Tang, Y., Qu, Y., 2021. Individual tree crown detection from high spatial resolution imagery using a revised local maximum filtering. Remote Sens. Environ. 258, 112397. http://dx.doi.org/10.1016/j.rse.2021.112397.

Zhen, Z., Quackenbush, L.J., Stehman, S.V., Zhang, L., 2015. Agent-based region growing for individual tree crown delineation from airborne laser scanning (ALS) data. Int. J. Remote Sens. 36 (7), 1965–1993. http://dx.doi.org/10.1080/01431161.2015.1030043.

Zhen, Z., Quackenbush, L., Zhang, L., 2016. Trends in automatic individual tree crown detection and delineation—Evolution of LiDAR data. Remote Sens. 8 (4), 333. http://dx.doi.org/10.3390/rs8040333.

Zhou, T., Popescu, S., Lawing, A., Eriksson, M., Strimbu, B., Bürkner, P., 2018. Bayesian and classical machine learning methods: A comparison for tree species classification with LiDAR waveform signatures. Remote Sens. 10 (2), 39. http://dx.doi.org/10.3390/rs10010039.